17th World Conference on Earthquake Engineering, 17WCEE
Sendai, Japan - September 13th to 18th 2020

EXPERIMENT TO ANALYSIS – DEFINING PERFORMANCE LIMIT-STATES FOR CFT COLUMNS

Y. Hori [(1)], D. Pettinga [(2)], Y. Suzuki[(3)], M. Nakashima[(4)]

[(1)] *Deputy Manager, Kobori Research Complex Inc., horiyus@kobori-takken.co.jp*
[(2)] *Technical Director, Holmes Consulting LP, didier.pettinga@holmesconsulting.co.nz*
[(3)] *General Manager, Kobori Research Complex Inc., y-suzuki@kobori-takken.co.jp*
[(4)] *President, Kobori Research Complex Inc., nakashima-masayoshi@kobori-takken.co.jp*

Abstract

CFT columns are widely applied to steel buildings in Japan, and recently have become more common in New Zealand for ductile two-way moment-frame construction. In Japan the design standard adopted for CFT columns is the *Recommendations for Design and Construction on Concrete Filled Steel Tubular Structures* published by Architectural Institute of Japan, while New Zealand has recently published AS/NZS 2327:2017 *Composite steel-concrete construction in buildings*, which for CFT design is closely aligned to Eurocode 4. Using these codes as examples, the development has been driven by a combination of theory and experimental observation, aimed at defining acceptable design approaches. However there is very little published information that defines suitable parameters for non-linear modelling of CFT columns, that would be suitable for general use in non-linear static or non-linear dynamic analyses. In this study the modeling parameters which determine the deterioration characteristics, and the seismic performance criteria that define the deformation capacity and strength degradation of CFT columns, according to ASCE41-17 definitions, are proposed for application in nonlinear analysis.

The development of the CFT specific parameters is an important step to improving the efficiency in application of this type of lateral-force resisting system. It will enable engineering design and analysis to take advantage of CFT column characteristics, such as the extended inelastic deformation capacity and the more gradual strength loss for deformations after reaching peak strength, which existing steel and concrete column definitions do not adequately capture.

Keywords: Concrete-filled tube; Moment-frame; Non-linear backbone; Performance Limit-State

1. Introduction

In Japan structural steel moment frame systems are often adopted for office-use buildings, with CFT (Concrete Filled Tube) columns being widely applied for these structures from mid-rise to high-rise buildings. In addition to the fact that CFT columns have good structural performance such as their high strength and deformation capacity, they are also economically beneficial because the amount of steel can be reduced compared to normal steel columns. In recent years, high tensile strength steel of 780 N/mm^2 and high compressive strength concrete of 150 N/mm^2 also have been applied[1]. The applicable range of CFT columns is becoming quite wide. In Japan, the design of CFT columns usually follows the guideline *Recommendations for Design and Construction of Concrete Filled Tubular Structures* published by the Architectural Institute of Japan (AIJ)[2]. This design guideline defines the critical rotation as the point which the bending moment is reduced by 5% from the maximum capacity. CFT columns are designed within the range that the response rotation is less than the critical rotation under seismic excitation.

Meanwhile in New Zealand, the number of steel structures in new buildings is increasing after the Canterbury earthquake sequence in 2010-2011, due to the fact that many reinforced concrete buildings were damaged in these earthquakes[3]. Many of those damaged buildings were reconstructed with steel moment frame or braced structures, and some of them have adopted CFT columns. The new composite design standard AS/NZS 2327:2017[4] was published recently so that the application of CFT columns is expected to spread in New Zealand. The previous design standard in New Zealand did not provide explicit account for CFT column design or analysis, and as such structural engineers had relied on overseas documents such as Eurocode 4[5], as an Alternative Solution in order to meet the intent of the New Zealand Building Code. The New Zealand Composite Structures Standard explicitly incorporates seismic design considerations, and generally follows Eurocode 4 for CFT column design, although with minor adjustments to suit the New Zealand Standards context and design approach. The composite stiffness factor is also adjusted, with the effective concrete stiffness contribution having a coefficient of 0.2. It is noted that the New Zealand Standards typically do not provide guidance for non-linear modelling of elements, and as such no information is provided for developing backbone curves or appropriate hysteresis representations of CFT column response.

One of the most frequently referred-to standards for performance-based seismic design is ASCE41-17[6]. Although it provides backbone curves and seismic performance criteria for structural steel, reinforced concrete, masonry and wooden structures, there is no clear definition of backbone curves and criteria for CFT structures. As with ASCE41-17, AS/NZS 2327:2017 and Eurocode 4 are also not set up to provide non-linear modeling parameters. Structural engineers who need non-linear modeling of CFT columns have likely used their own research to develop approximate backbone and hysteretic definitions, or have assumed that ASCE41-17 backbone definitions for well-detailed and Compact steel columns are appropriate, and likely conservative.

A lot of experiment studies have been conducted on CFT structures in Japan over the past few decades. Especially in the US-Japan joint structural experiment research on hybrid structures, conducted over five years from 1992 (Chairman of the technical coordination committee: Hiroyuki Aoyama, Professor Emeritus of the University of Tokyo), many experiments were completed on various specimens with different cross-sectional shapes, as well as a range of steel and concrete material types. Various loading protocols such as compression loading, bending-shear loading in monotonic or cyclic conditions were part of these investigations. The results of the project were reflected in the AIJ design guideline for CFT structures and nowadays widely referred in Japan. However, since the Japanese seismic design procedure specifies that the deterioration of structural elements is basically not allowed under extremely rare earthquakes, the structural performance of CFT columns is defined only in the range where the strength loss is not significant (no more than 5% reduction from the peak moment capacity) in the guideline. In countries other than Japan, the seismic force is often based on Maximum Considered Earthquake which has the return period of approximately 1,000 years to 2,500 years and the deterioration is usually allowed to occur so that the structural performance defined in the AIJ design guideline would not be sufficient.

In this paper, the backbone curve of CFT columns is developed according to the definition of ASCE41-17 including the strength deterioration based on the experiment which was conducted in the US-Japan joint research project. The limit state and modeling recommendation for the performance-based seismic design are also proposed, which can also be applied in-line with NIST 2017 (Part IIa) guidance[8].

2. Reference experiment outline

With reference to the papers describing the structural performance experiments of CFT columns conducted in the US-Japan joint structural experiment research on hybrid structures[9~15], a new backbone curve of CFT columns is proposed. In this section, the outline of the experiment is shown by citing these papers.

The test specimen is a single column shown in Fig.1, and both ends of the columns are restrained by rigid stubs. After the axial force is introduced in the column, the upper stub is loaded so as to generate the inverse symmetric bending moment in the column. The parameters of test specimen are section shape (rectangular and round Hollow Structural Section), tensile strength of steel plates (400N/mm^2, 600 N/mm^2 and 800 N/mm^2), compressive strength of the concrete fill (40N/mm^2 and 90N/mm^2) and thickness of steel plates. The thickness

of steel plates is designed to match FA rank which has sufficient plastic deformation capacity or FC rank which has the low plastic deformation capacity according to *Structural Regulations for Buildings*[16] . As for the axial force introduced in the specimen, the constant axial force of 0.4 times the axial compression strength is considered for the all specimens. Specimens loaded with variable axial force are also described in the original paper, but they are not used for the backbone curve setting in this study in order to focus on the behavior under the constant axial force as a first step of the study. Table 1 and 2 are the lists of the specimens used in this study, 12 of them are the rectangular HSS specimens, and 9 of them are round HSS specimens.

α_R and α_C in Table 1 and 2 are the normalized width-thickness ratio of rectangular HSS and the normalized diameter-thickness ratio of round HSS, respectively. ${}_sE$ is Young's modulus of steel in the following equations.

$$\alpha_R = \frac{D_R}{t}\sqrt{\frac{{}_s\sigma_y}{{}_sE}} \tag{1}$$

$$\alpha_C = \frac{D_C}{t}\frac{{}_s\sigma_y}{{}_sE} \tag{2}$$

The horizontal loading pattern is cyclic loading, where the rotation of specimens in each cycle is 0.0025, 0.005, 0.0075, 0.01 twice, 0.015 twice, 0.01, 0.02 twice, 0.03, 0.04. The final cycle is monotonic loading until the bending moment decreases by 80% of maximum bending moment or the rotation reaches 0.06.

Table 1 – Specimens list (rectangular HSS)

	D_R (mm)	t (mm)	D_R/t	${}_s\sigma_y$ (N/mm^2)	${}_c\sigma_B$ (N/mm^2)	L (mm)	N (kN)	α_R	Cited from
SR4A4C	210	5.80	36.2	294	39.2	1260	1162	1.32	[9],[11]
SR4C4C	210	4.50	46.7	276	39.2	1260	1021	1.71	[9],[11]
SR6A4C	211	8.83	23.9	536	39.3	1261	1959	1.19	[9],[12]
SR6C4C	211	5.95	35.5	540	39.3	1261	1545	1.79	[9],[12]
SR8A4C	178	9.45	18.8	824	42.3	1080	2576	1.20	[9],[14]
SR8C4C	180	6.66	27.0	851	42.3	1081	2003	1.71	[9],[14]
SR4A9C	210	5.80	36.2	294	88.2	1260	1895	1.32	[9],[11]
SR4C9C	209	4.50	46.4	276	88.2	1260	1791	1.71	[9],[11]
SR6A9C	211	8.83	23.9	536	88.3	1262	2649	1.19	[9],[12]
SR6C9C	210	5.95	35.3	540	93.7	1261	2368	1.79	[9],[12]
SR8A9C	179	9.45	18.9	824	94.5	1080	3077	1.20	[9],[14]
SR8C9C	180	6.66	27.0	851	94.5	1081	2540	1.71	[9],[14]

Table 2 – Specimens list (round HSS)

	D_C (mm)	t (mm)	D_C/t	${}_s\sigma_y$ (N/mm^2)	${}_c\sigma_B$ (N/mm^2)	L (mm)	N (kN)	α_C	Cited from
SC4A4C	241	4.70	51.3	338	39.2	1446	1034	0.07	[9],[11]
SC6A4C	241	9.00	26.8	508	35.5	1446	1809	0.06	[9],[13]
SC6C4C	238	4.52	52.7	530	35.5	1428	1462	0.13	[9],[13]
SC8A4C	161	9.12	17.7	806	35.5	966	1612	0.07	[9],[15]
SC4A9C	238	4.70	50.6	338	88.2	1428	1784	0.07	[9],[11]
SC6A9C	241	9.00	26.8	508	84.4	1446	2567	0.06	[9],[13]
SC6C9C	240	4.52	53.1	530	84.4	1440	2086	0.13	[9],[13]
SC8A9C	161	9.12	17.7	806	93.9	966	1988	0.07	[9],[15]
SC8C9C	160	4.76	33.6	785	93.9	960	1347	0.13	[9],[15]

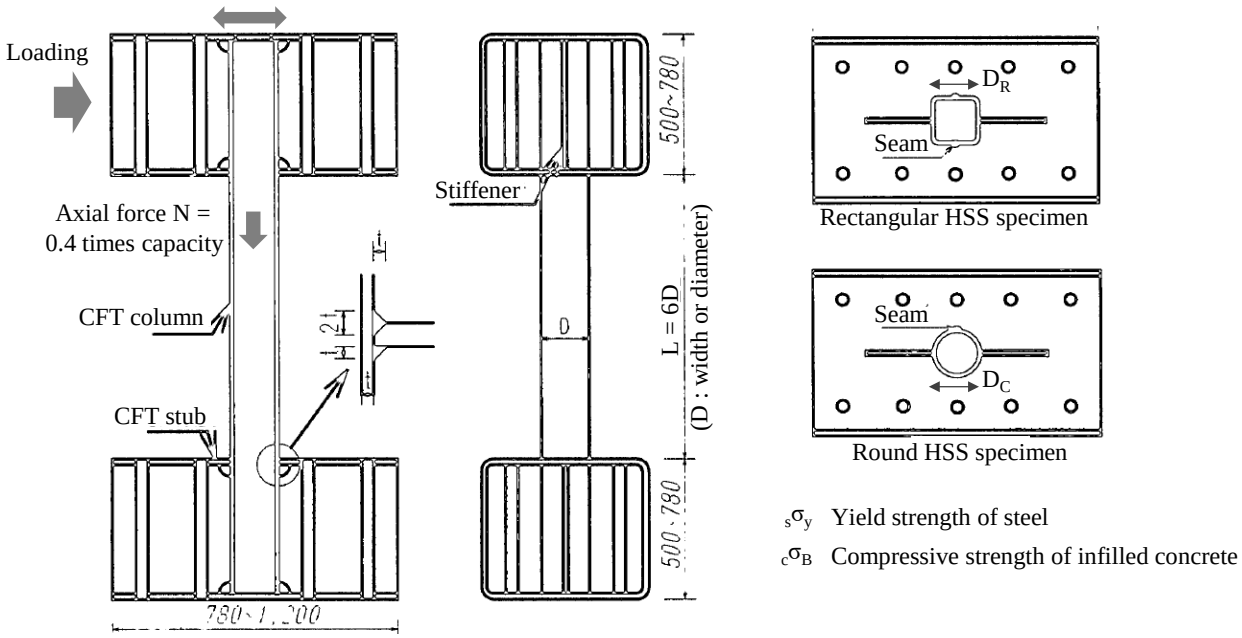

Fig.1 – Specimen configuration (cited from [9] and modified)

3. Idealized force-deformation curve developed from the experimental result

The rotation-bending moment relationship of each specimen is read from the original paper, and then the backbone curve is set according to the definition of ASCE41-17. In ASCE41-17, the envelope curve is set so as to envelope the maximum deformation point in each cycle, then the parameters of control points of idealized force-deformation curve are developed. The envelope curves are already given in the original papers, so the idealized backbone curves are developed in this study.

Fig.2 shows the idealized force-deformation curve per ASCE41-17 and the procedure for how to fit the envelope curve from cyclic test to the idealized force-deformation curve.

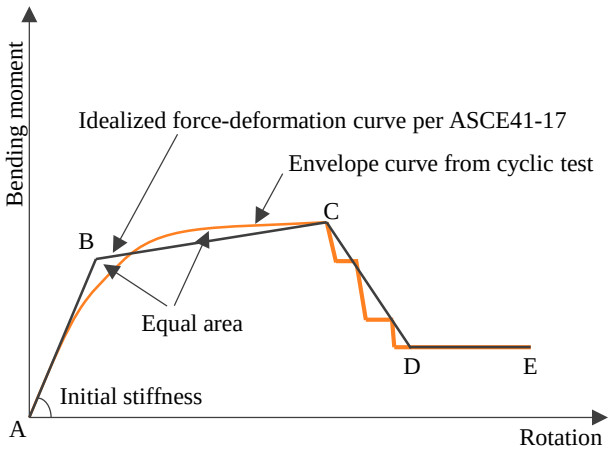

- Point A: Origin.
- Point B: Elastic limit. The slope from point A to point B is assumed to be equal to the initial stiffness of the experiment. Point B is determined to make the area surrounded by point A, B and C is approximately equal to the area of envelope curve to point C.
- Point C: Maximum capacity. The bending moment at this point is already given in the original paper so rotation is read in this study.
- Point D: Stable point. The moment capacity reduction ends and keeps stable.
- Point E: Maximum deformation. Loading range in the experiment.

Fig.2 – Idealized force-deformation curve per ASCE41-17

Note that the rotation read from the experimental results includes not only the deformation of columns themselves but also the local deformation of the test pieces between the column and the loading stubs. According to the structural performance test of a cross-shaped specimen consisting of CFT column and steel beam[17], it is known that the initial stiffness of CFT columns can be accurately expressed by the simple addition of steel section and infilled concrete section assuming Bernoulli-Euler theory. Although some design standards apply the correction factor to concrete section in order to achieve the effective stiffness against bending deformation observed in the experiment (0.6 in Eurocode 4 and 0.2 in AS/NZS2327:2017), the difference between the initial stiffness k_1 obtained from the cross-sectional parameters and the initial stiffness $k_1{}'$ of the experimental result is subtracted from the rotation θ' read from the experimental result in order to obtain the rotation θ due to the columns deformation. M stands for the bending moment of the specimen at the deformation of θ′.

$$\theta = \theta' - M\left(\frac{k_1 - k_1{}'}{k_1 k_1{}'}\right) \tag{3}$$

The initial stiffness k_1 is obtained from the cross-sectional parameter by following equations.

$$k_1 = \frac{6\ {}_eE\ {}_eI}{L(1+\eta)} \tag{4}$$

$$\eta = \frac{12\ {}_eE\ {}_eI}{L^2\ {}_eG\ {}_eA_S} \tag{5}$$

${}_eE$ and ${}_eG$ are the equivalent Young's modulus and shear modulus of the steel / concrete composite section, and usually use the value of either steel or infilled concrete. ${}_eI$ and ${}_eA_s$ are the equivalent moment of inertia and shear cross section of the CFT column, which are obtained by simple addition of steel and concrete considering the elastic stiffness. No correction factor is applied to the concrete section here. L is the length of column.

Fig. 3 shows the idealized backbone curve of the rectangular HSS specimens and Fig.4 shows that of the round HSS specimens, respectively. In the rectangular HSS specimens, the strength loss is observed after local buckling has occurred. The strength loss is not observed in the round HSS specimens except for the specimens with 800N/mm^2 tensile strength steel. It is reported that the cracks are developed and progressed in the weld heat affected zone between the column and the loading stubs in these specimens (SC8A4C, SC8A9C and SC8C9C), so that the results of these specimens are excluded when evaluating point D, and no strength loss is considered for the round HSS columns. Also, SR4A9C and SR4C9C specimens show the radical strength loss under the same deformation cycles. These specimens have the combination of low strength steel (400N/mm^2) and high compressive strength concrete (90N/mm^2) and they are not realistic in actual application, so they are also excluded from the evaluation of point D.

Table 3 and 4 shows the rotation ratio of point C and D to point B, and the bending moment ratio of point B, C and D to the calculated bending moment capacity M_p. The bending moment capacity M_p of each specimen follows the AIJ design guideline. The confined effect between steel and infilled concrete is not considered for the rectangular HSS specimens, but it is considered for the round HSS specimens.

Fig. 5 shows the relationship between the normalized width-thickness ratio α_R, infilled concrete compressive strength ${}_c\sigma_B$ and parameters on idealized backbone curve. Generally speaking, the smaller the normalized width-thickness ratio, the higher the deformation capacity tends to be so that it is possible to improve the deformation capacity by avoiding local buckling. The bending moment capacity M_p calculated from the AIJ design guideline approximately corresponds to M_B and M_C, and is about 20% higher than M_p. The stable moment capacity has a relatively high correlation with the normalized width-thickness ratio α_R.

The smaller the normalized width-thickness ratio is, the higher the stable moment is, that is, the smaller the strength deterioration is.

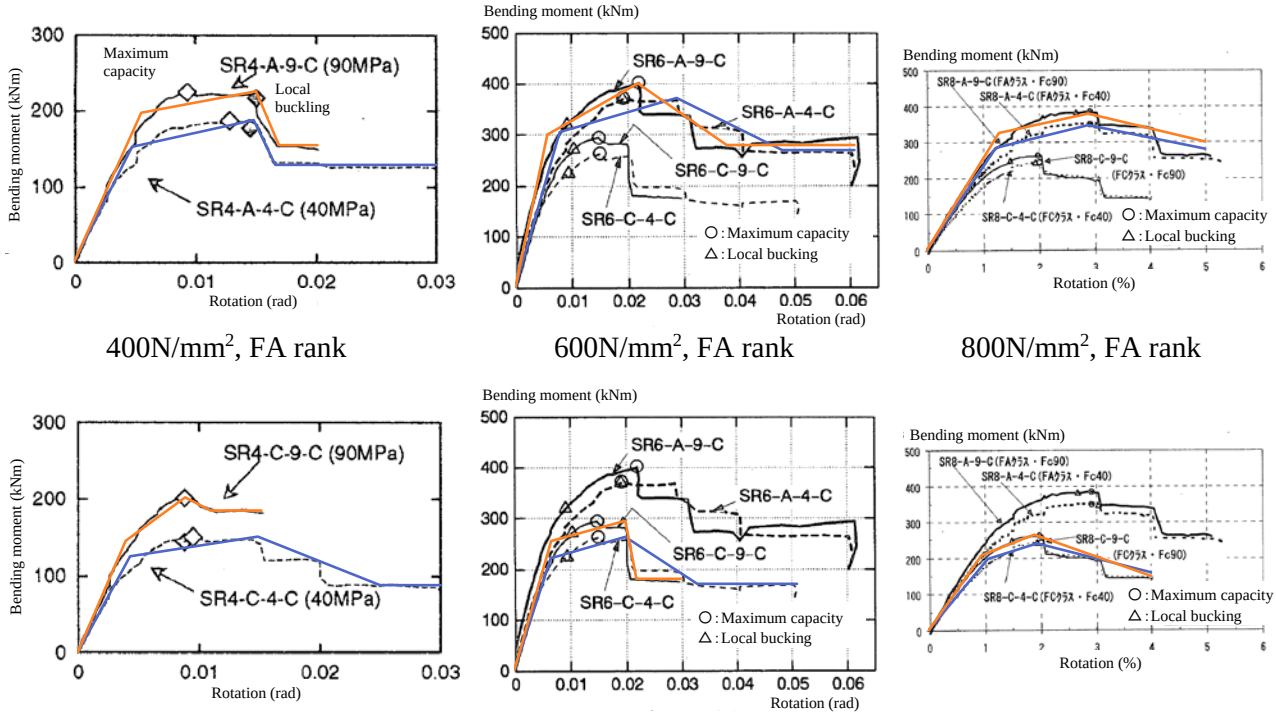

400N/mm^2, FA rank | 600N/mm^2, FA rank | 800N/mm^2, FA rank

400N/mm^2, FC rank | 600N/mm^2, FC rank | 800N/mm^2, FC rank

Fig.3 - Idealized backbone curve (rectangular HSS)

(Cited from [11][12][14] and modified)

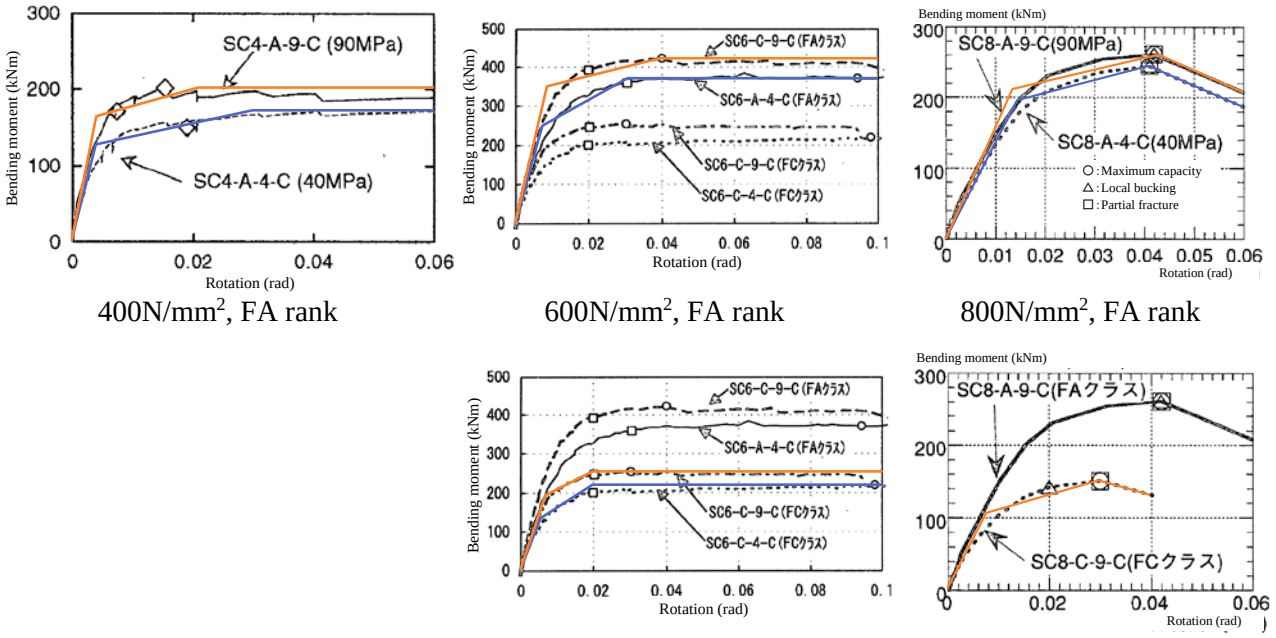

400N/mm^2, FA rank | 600N/mm^2, FA rank | 800N/mm^2, FA rank

600N/mm^2, FC rank | 800N/mm^2, FC rank

Fig.4 - Idealized backbone curve (round HSS)

(Cited from [11][13][15] and modified)

Table 3 – Idealized backbone curve parameters (rectangular HSS)

	Rotation (%)			Bending moment (kNm)			Rotation ratio		Bending moment ratio		
	θ_B	θ_C	θ_D	M_B	M_C	M_D	θ_C/θ_B	θ_D/θ_B	M_B/M_p	M_C/M_p	M_D/M_p
SR4A4C	0.33	1.30	1.54	152	187	128	3.96	4.69	1.18	1.45	0.99
SR4C4C	0.30	1.33	2.41	126	151	88	4.39	7.95	1.17	1.41	0.82
SR6A4C	0.53	2.58	4.57	305	373	270	4.83	8.55	1.07	1.31	0.95
SR6C4C	0.47	1.78	3.16	221	263	170	3.82	6.78	1.02	1.22	0.79
SR8A4C	0.74	2.28	4.50	282	345	280	3.10	6.11	0.98	1.19	0.97
SR8C4C	0.59	1.38	3.62	197	240	160	2.33	6.11	0.83	1.02	0.68
SR4A9C	0.40	1.33	1.58	197	225	154	3.32	3.93	1.12	1.28	0.88
SR4C9C	0.33	0.80	(1.02)	146	202	(185)	2.40	(3.05)	0.97	1.34	(1.23)
SR6A9C	0.50	2.11	3.74	301	402	280	4.19	7.43	0.90	1.21	0.84
SR6C9C	0.51	1.83	2.10	255	295	180	3.55	4.07	0.96	1.11	0.68
SR8A9C	0.80	2.32	4.54	323	377	300	2.91	5.69	0.98	1.15	0.91
SR8C9C	0.59	1.44	3.74	207	264	150	2.43	6.31	0.76	0.96	0.55

Table 4 – Idealized backbone curve parameters (round HSS)

	Rotation (%)			Bending moment (kNm)			Rotation ratio		Bending moment ratio		
	θ_B	θ_C	θ_D	M_B	M_C	M_D	θ_C/θ_B	θ_D/θ_B	M_B/M_p	M_C/M_p	M_D/M_p
SC4A4C	0.35	2.93	-	127	172	-	8.42	-	0.89	1.20	-
SC6A4C	0.51	2.75	-	249	371	-	5.39	-	0.81	1.21	-
SC6C4C	0.38	1.71	-	134	220	-	4.45	-	0.74	1.22	-
SC8A4C	1.09	3.66	-	196	245	-	3.36		1.02	1.28	-
SC4A9C	0.43	2.13	-	164	202	-	4.92	-	0.88	1.08	-
SC6A9C	0.68	3.77	-	350	422	-	5.51	-	0.99	1.19	-
SC6C9C	0.50	1.75	-	193	254	-	3.48	-	0.80	1.06	-
SC8A9C	1.14	4.05	-	212	261	-	3.56	-	1.02	1.25	-
SC8C9C	0.78	3.01	-	106	151	-	3.85	-	0.82	1.17	-

Eq. (6) and (7) are the result of a linear regression of the slopes and intercepts of the approximate linear line in Fig.5 which are expressed as a function of normalized width-thickness ratio α_R and infilled concrete compressive strength ${}_c\sigma_B$.

$$\begin{cases} \theta_B = M_B/k_1 \\ \theta_C = \{(-0.00786\ {}_c\sigma_B - 0.495)\alpha_R + (-0.000377\ {}_c\sigma_B + 4.96)\}\theta_B \\ \theta_D = \{(-0.0614\ {}_c\sigma_B + 2.77)\alpha_R + (0.0740\ {}_c\sigma_B + 3.26)\}\theta_B \\ \theta_E = 0.04 \end{cases} \quad (6)$$

$$\begin{cases} M_B = \{(-0.00131\ {}_c\sigma_B - 0.0345)\alpha_R + (0.0000579\ {}_c\sigma_B + 1.17)\}M_p \\ M_C = \{(0.000504\ {}_c\sigma_B - 0.169)\alpha_R + (-0.00259\ {}_c\sigma_B + 1.59)\}M_p \\ M_D = \{(-0.00140\ {}_c\sigma_B - 0.326)\alpha_R + (-0.000507\ {}_c\sigma_B + 1.45)\}M_p \\ M_E = M_D \end{cases} \quad (7)$$

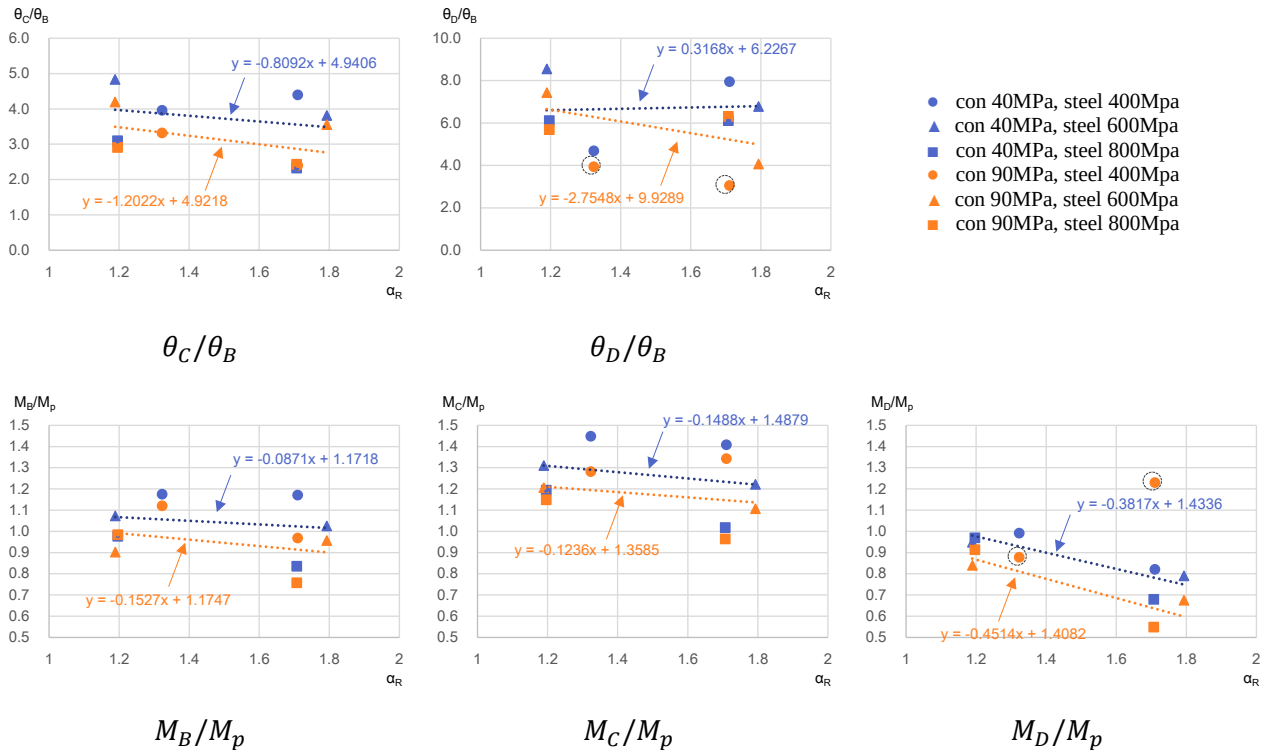

Fig.5 – Parameter identification of idealized backbone curve (rectangular HSS)

Note: the circled plots are not used for linear regression.

Fig. 6 shows the relationship between the normalized diameter-thickness ratio α_C, infilled concrete compressive strength ${}_c\sigma_B$ and parameters on idealized backbone curve. In the same manner as the rectangular HSS specimens, the smaller the normalized diameter-thickness ratio, the higher the deformation capacity tends to be. M_C is higher than the bending moment capacity M_p calculated from the AIJ design guideline by approximately 20%. Regarding round HSSs, since the strength loss is not observed in the experiment, the bending moment at point D and E is the same as that of point C.

Eq. (8) and (9) are the result of a linear regression of the slopes and intercepts of the approximate linear line in Fig. 6 which are expressed as a function of normalized diameter-thickness ratio α_C and infilled concrete compressive strength ${}_c\sigma_B$ as well as the rectangular HSS.

$$\begin{cases} \theta_B = M_B/k_1 \\ \theta_C = \{(0.0186\ {}_c\sigma_B - 19.6)\alpha_C + (-0.0213\ {}_c\sigma_B + 7.82)\}\theta_B \\ \theta_E = 0.06 \end{cases} \tag{8}$$

$$\begin{cases} M_B = \{(0.000667\ {}_c\sigma_B - 2.53)\alpha_C + (0.00108\ {}_c\sigma_B + 1.03)\}M_p \\ M_C = \{(-0.0161\ {}_c\sigma_B + 0.457)\alpha_C + (-0.00000799\ {}_c\sigma_B + 1.24)\}M_p \\ M_E = M_C \end{cases} \tag{9}$$

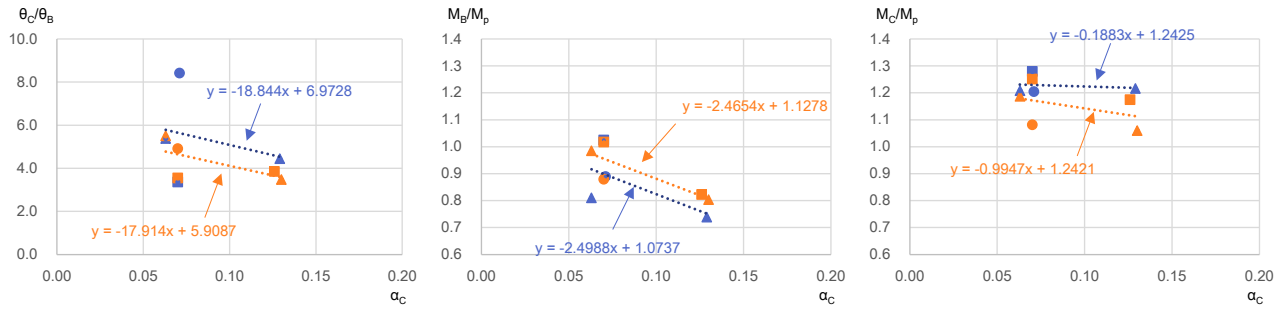

θ_C/θ_B M_B/M_p M_C/M_p

Fig.6 – Parameter identification of idealized backbone curve (round HSS)

Fig. 7 shows the comparison between the hysteresis loop obtained from the experiment and idealized backbone curve calculated by Eq. (6) and (7) for the rectangular HSS specimens, and also Fig.8 shows the comparison between the hysteresis loop obtained from the experiment, and idealized backbone curve calculated by Eq. (8) and (9) for the round HSS specimens as well. The proposed backbone curve generally envelopes the experimental result so that it can be said that the proposed backbone curves are suitably accurate. The applicable ranges of the proposed backbone curve are as follows;

Section shape	:	Rectangular HSS or round HSS
Tensile strength of steel	:	400N/mm^2 to 800 N/mm^2 for rectangular HSS 400N/mm^2 to 600 N/mm^2 for round HSS
Width-thickness ratio of steel	:	19 to 46 for rectangular HSS
Diameter-thickness ratio of steel	:	18 to 52 for round HSS
Compressive strength of infilled concrete	:	40N/mm^2 to 90N/mm^2
Length of column	:	L/D is around 6.0
Axial force in column	:	N/N$_0$ is around 0.4 (N$_0$ is the axial capacity of column)
Material combination	:	Combination of 400N/mm^2 steel and 90N/mm^2 concrete is not applicable

4. Performance limit state

Table 5 shows the rotation of each performance limit state which are evaluated based on the experimental result and the proposed backbone curve. Immediate Occupancy is defined as the range which has some margin to avoid local buckling, Life Safety is defined as the range not to have local buckling, and Collapse prevention is defined as the range which the deformation capacity is confirmed in the experiment.

Table 5 – Performance limit state

	Immediate Occupancy	Life Safety	Collapse Prevention
Rectangular HSS	75% of θ_C	θ_C of Eq.(6)	0.04
Round HSS	75% of θ_C	θ_C of Eq.(8)	0.06

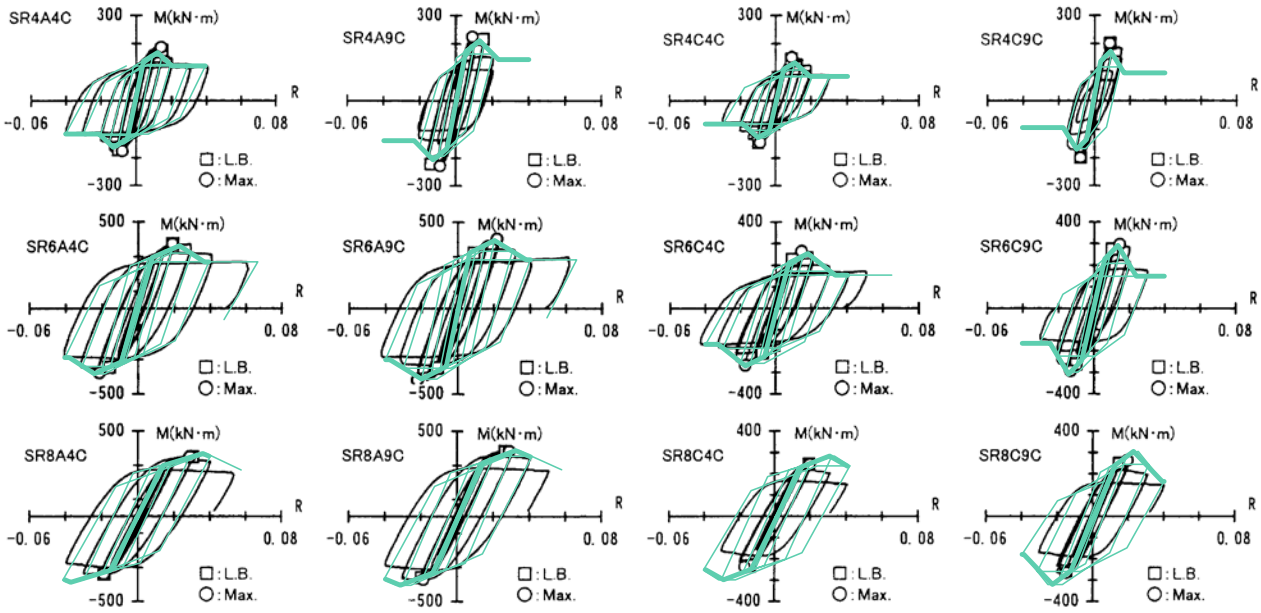

Backbone curve per Eq.(6) and (7) Hysteresis loop by Perform 3D

Fig.7 – The proposed backbone curve and hysteresis loop by Perform 3D (rectangular HSS)

(Cited from [9] and modified)

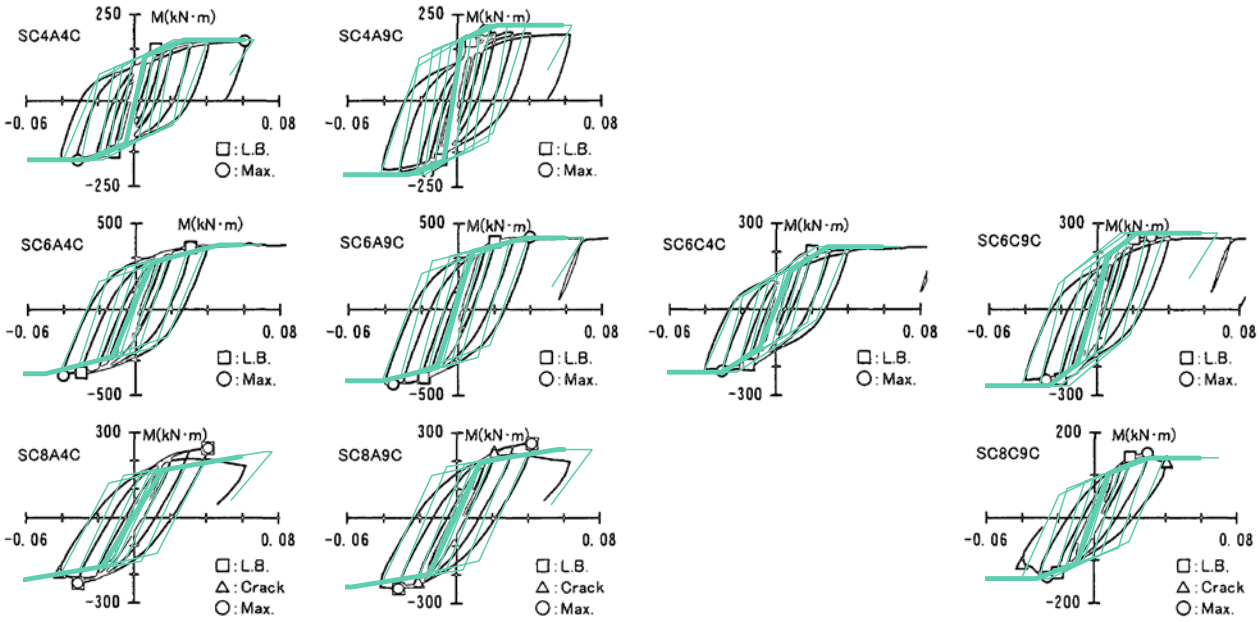

Backbone curve per Eq.(8) and (9) Hysteresis loop by Perform 3D

Fig.8 – The proposed backbone curve and hysteresis loop by Perform 3D (round HSS)

(Cited from [9] and modified)

5. Perform 3D modeling recommendation

For the non-linear dynamic response analysis, the hysteresis loop characteristics is needed in addition to the proposed backbone curve by Eq. (6) and (7) or Eq. (8) and (9). Table 5 and 6 show the non-linear modeling recommendations if the non-linear dynamic response analysis software Perform 3D[18], which is widely used in the framework of performance-based seismic design all over the world, is used. Also, the hysteresis loops developed by Perform 3D are shown in Fig.8.

Table 5 – Modeling recommendation in Perform 3D (rectangular HSS)

Strength Loss	Cyclic Degradation		Y	U	L	R	X
Yes	YULRX	Energy factor	1.0	1.0	0.8	0.8	0.8

Table 6 – Modeling recommendation in Perform 3D (round HSS)

Strength Loss	Cyclic Degradation		Y	1	2	3	X
No	YX+3	Deformation	-	θ_C	*1	*1	-
		Energy factor	1.0	1.0	0.6	0.6	0.6

*1 any point between θ_C and θ_E

6. Conclusion

Idealized backbone curves of CFT columns with rectangular HSSs or round HSSs are developed based on past experimental data. The backbone curves are formulated using the normalized width-thickness ratio, or the normalized diameter-thickness ratio, along with concrete compressive strength as parameters. It is confirmed that they are suitably accurate in order to envelope the hysteresis loops of the experimental data. Further to this, the modeling parameters for the non-linear dynamic response analysis software Perform 3D are proposed.

The proposed backbone curve is developed based on a limited number of specimens. Although the steel material strength, steel plate thickness and concrete compressive strength are taken into account as parameters, the effect of the column length and the axial force are not included in the equations. In applying the documented approach, it is necessary to pay attention to the applicable ranges, based on the reference data.

7. Acknowledgement

In writing this paper, we refer to the experimental results and papers conducted in the US-Japan joint structural experiment research on hybrid structures conducted for five years from 1992 (Chairman of the technical coordination committee: Hiroyuki Aoyama, Professor Emeritus of the University of Tokyo). We would like to express our sincere gratitude to everyone who was involved in the project.

8. References

[1] Matsumoto S, Komuro T, Kawamoto S, Hosozawa O, Morita K (2012): Structural Design of an Ultra High-rise Building Using Concrete Filled Tubular Column with Ultra High Strength Materials, 15th World Conference on Earthquake Engineering.

[2] Architectural Institute of Japan (2008): Recommendations for Design and Construction of Concrete Filled Steel Tubular Structures (in Japanese)

[3] Bruneau M, MacRae G (2017): RECONSTRUCTING CHIRISTCHURCH: A Seismic Shift in Building Structural Systems, Quake Centre, Canterbury University

[4] AS/NZS 2327:2017 (2017): Australian / New Zealand Standard Composite structures – Composite steel-concrete construction in buildings, Standards Australia and Standards New Zealand

[5] EN1994-1-1 (2007): Eurocode 4: Design of composite steel and concrete structures – Part 1-1: General rules and rules for buildings, European Committee for Standardization, Brussels

[6] ASCE/SEI 41-17 (2017): Seismic Evaluation and Retrofit of Existing Buildings, American Society of Civil Engineering, Reston, Virginia

[7] Nishiyama I, Yamanouchi H, Aoyama H (1999): U.S.-Japan Cooperative Earthquake Engineering Research on Composite and Hybrid Structures, AIJ J. Technology, Des No.9, 107-110, Architectural Institute of Japan (In Japanese)

[8] NIST (2017): Guidelines for Nonlinear Structural Analysis for Design of Buildings Part IIa – Steel Moment Frames, GCR 17-917-46v2, prepared by the Applied Technology Council for the National Institute of Technology and Standards, Gaithersburg, Maryland.

[9] Fujimoto T, Mukai A, Nishiyama I, Inai E, Kai M, Tokinoya H, Baba T, Fukumoto T, Mori K, Sakino K, Morino S (1998): Shear-Flexural Behavior of Concrete Filled Steel Tubular Beam-Columns Using High Strength Materials, J. Struct. Constr. Eng, AIJ No. 509, 167-174, Architectural Institute of Japan (In Japanese)

[10] Mukai A, Yoshioka K, Nishiyama I, Morino S (1996): U.S.-Japan Cooperative Earthquake Engineering Research on Composite and Hybrid Structures (CFT-9) Shear-Flexural Behavior of Concrete-Filled Steel Tubular Columns Part1 Test Program, Summaries of technical papers of Annual Meeting, Architectural Institute of Japan, 22512,1023-1024 (In Japanese)

[11] Mori K, Fukumoto N (1996): U.S.-Japan Cooperative Earthquake Engineering Research on Composite and Hybrid Structures (CFT-11) Shear-Flexural Behavior of Concrete-Filled Steel Tubular Columns Part3 Test Results on Circular CFT using 780Nmm^2 Tensile Strength Steel, Summaries of technical papers of Annual Meeting, Architectural Institute of Japan, 22514,1027-1028 (In Japanese)

[12] Kai M, Nishinaga M, Nishino K (1996): U.S.-Japan Cooperative Earthquake Engineering Research on Composite and Hybrid Structures (CFT-12) Shear-Flexural Behavior of Concrete-Filled Steel Tubular Columns Part4 Test Results on Rectangular CFT using 590N/mm^2 Tensile Strength Steel, Summaries of technical papers of Annual Meeting, Architectural Institute of Japan, 22515,1029-1030 (In Japanese)

[13] Fujimoto T, Baba T, Mukai A, Nishiyama I (1996): U.S.-Japan Cooperative Earthquake Engineering Research on Composite and Hybrid Structures (CFT-13) Shear-Flexural Behavior of Concrete-Filled Steel Tubular Columns Part5 Test Results on Circular CFT using 780N/mm^2 Tensile Strength Steel, Summaries of technical papers of Annual Meeting, Architectural Institute of Japan, 22516,1031-1032 (In Japanese)

[14] Inai E, Tabata K, Okada K (1996): U.S.-Japan Cooperative Earthquake Engineering Research on Composite and Hybrid Structures (CFT-14) Shear-Flexural Behavior of Concrete-Filled Steel Tubular Columns Part6 Test Results on Rectangular CFT using 780N/mm^2 Class Steel, Summaries of technical papers of Annual Meeting, Architectural Institute of Japan, 22517,1032-1033 (In Japanese)

[15] Fukumoto T, Inoue T (1996): U.S.-Japan Cooperative Earthquake Engineering Research on Composite and Hybrid Structures (CFT-15) Shear-Flexural Behavior of Concrete-Filled Steel Tubular Columns Part7 Test Results on Circular CFT using 780N/mm^2 Tensile Strength Steel, Summaries of technical papers of Annual Meeting, Architectural Institute of Japan, 22518,1033-1034 (In Japanese)

[16] Building Center Japan (1994): Structural Regulations for Buildings (In Japanese)

[17] Inai E, Tabata K (1998): U.S.-Japan Cooperative Earthquake Engineering Research on Composite and Hybrid Structures (CFT-26) Experiment of CFT Column-Steel Beam Connections Part 2 Behavior of Rectangular CFT Connections I, Summaries of technical papers of Annual Meeting, Architectural Institute of Japan, 22607,1211-1212 (In Japanese)

[18] Computers and Structures Inc : Perform 3D (https://www.csiamerica.com/products/perform-3d)

